Inhibition of nonlinear acoustic cavitation dynamics in liquid CO2

Inhibition of nonlinear acoustic cavitation dynamics in liquid CO_2

Maikel M. van Iersel
Process Development Group, Department of Chemical Engineering and Chemistry, Eindhoven University of Technology, P.O. Box 513, 5600 MB Eindhoven, The Netherlands

Jeroen Cornel[a)]
Institute of Process Engineering, ETH Swiss Federal Institute of Technology Zurich, Sonneggstrasse 3, CH-8092 Zurich, Switzerland

Nieck E. Benes[b)] and Jos T. F. Keurentjes
Process Development Group, Department of Chemical Engineering and Chemistry, Eindhoven University of Technology, P.O. Box 513, 5600 MB Eindhoven, The Netherlands

(Received 28 November 2006; accepted 28 December 2006; published online 13 February 2007)

The authors present a model to study ultrasound-induced cavitation dynamics in liquid carbon dioxide (CO_2), which includes descriptions for momentum, mass, and energy transport. To assist in the interpretation of these results, numerical simulations are presented for an argon cavity in water. For aqueous systems, inertia effects and force accumulation lead to a nonlinear radial motion, resulting in an almost adiabatic compression of the cavity interior. The simulations for liquid CO_2 suggest that transport limitations impede nonlinear cavitation dynamics and the corresponding temperature rise. Consequently, in liquid CO_2 the ultrasound-induced formation of radicals appears improbable. © *2007 American Institute of Physics*. [DOI: 10.1063/1.2434962]

I. INTRODUCTION

Irradiation of a liquid with high intensity ultrasound is known to enhance or alter a wide variety of chemical reactions.[1,2] It has been reported that ultrasound successfully increases conversion, changes reaction pathways, initiates reactions, and accelerates mixing.[3] These physical and chemical effects of ultrasound predominantly arise from acoustic cavitation. Acoustic cavitation is the growth and subsequent contraction of a cavity in a liquid induced by pressure variations from a sound wave. During the contraction of the cavity, its contents can be almost adiabatically heated, leading to hot spots in the liquid in which temperatures of ~5000 K and pressures of several hundreds of bars can be reached.[1] These conditions enable demanding (sono)chemistry, while the macroscopically observable properties of the system remain unchanged.

Research in sonochemistry has evolved over the last decades. Up to now the focus has been on aqueous systems, e.g., for waste water treatment purposes.[4] In this work, acoustic cavitation in liquid CO_2 is investigated. In addition to its chemical inertness, CO_2 has a relatively high gas solubility.[5] This implies an increase in the number of cavitation nuclei and hence in the number of hot spots. Furthermore, the physicochemical properties of CO_2 are relatively easily tunable with small variations in pressure and temperature. In view of these inherent advantages, Kuijpers *et al.* experimentally investigated acoustic cavitation in liquid CO_2.[6] Since then, several other experimental studies of acoustic cavitation in high-pressure CO_2 have been conducted, in which ultrasound enhanced mass transfer.[7,8] To our knowledge, however, cavitation-induced radicalization has not been demonstrated in these types of systems. Accordingly, preliminary experiments have been performed in a high-pressure ultrasound reactor to study the radicalization of methane in liquid CO_2. Although the experimental conditions have been varied extensively, dissociation of methane could not be confirmed by gas chromatographic analysis of the reaction mixture. It is unclear whether this indicates milder hot-spot conditions in liquid CO_2 compared to aqueous systems. Numerical modeling studies, in which the governing processes are captured, can reveal whether "soft" cavitation is inherent for liquid CO_2.

Several models have been proposed in literature to describe cavitation dynamics.[9–11] Starting from these models, we have developed a comprehensible single-cavity dynamics model to study acoustic cavitation in liquid CO_2.

II. CAVITY DYNAMICS MODEL

A small preexisting cavity in an unbounded liquid is set into radial motion by applying a uniform ultrasonic field. The cavity remains spherical and fixed during this oscillation and the effect of bubble-bubble interactions, e.g., coalescence, is neglected. During contraction of the cavity, high temperatures can be obtained and chemical reactions take place. Although these reactions substantially influence the temperature rise, they are not incorporated into the model.

Since the cavity is small compared to the wavelength of the applied sound field, the cavity and its surrounding liquid are considered spatially uniform, except for thin boundary layers in which pressure and temperature vary as a function

[a)]Current address is given.
[b)]Author to whom correspondence should be addressed. Tel.: +31 40 247 5445; FAX: +31 40 244 6104. Electronic mail: n.e.benes@tue.nl

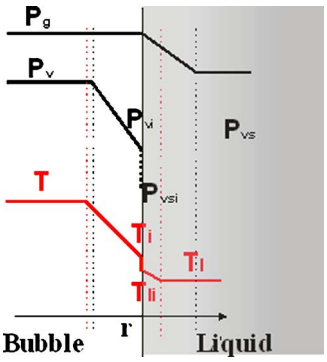

FIG. 1. Schematic representation of pressure and temperature profiles for the collapse phase. The dotted lines denote boundary layers.

of the radial distance r (Fig. 1). In the following sections, the governing equations for the cavity dynamics model are presented.

A. Equation of motion

The radial dynamics of a spherical boundary in a liquid is frequently described using the Rayleigh-Plesset equation,[12,13]

$$R\ddot{R} + \frac{3}{2}\dot{R}^2 = \frac{1}{\rho_l}[P_l - P_\infty]. \tag{1}$$

Here, R is the radius of the cavity, $\dot{R}$ is the cavity wall velocity, $\ddot{R}$ is the acceleration of the cavity wall, P_l is the pressure at the interface, P_∞ is the pressure infinitely far from the cavity, and ρ_l is the density of the liquid. The pressure at the interface is related to the pressure inside the cavity, P_b, using

$$P_l = P_b - \frac{2\sigma}{R} - 4\mu\frac{\dot{R}}{R}, \tag{2}$$

where σ is the surface tension and μ is the dynamic viscosity of the surrounding liquid. The cavity is set into radial motion by superimposing a sinusoidal acoustic pressure field on the hydrostatic pressure,

$$P_\infty = P_h - P_a \sin(2\pi f t). \tag{3}$$

Here, P_h is the hydrostatic pressure and P_a and f represent the amplitude and frequency of the ultrasonic field, respectively. To account for the effect of sound radiation and liquid compressibility, the Rayleigh-Plesset equation is extended to the Keller-Miksis formulation,[14]

$$\rho_l\left(1 - \frac{\dot{R}}{C}\right)R\ddot{R} + \frac{3}{2}\rho_l\left(1 - \frac{\dot{R}}{3C}\right)\dot{R}^2 = \left(1 + \frac{\dot{R}}{C}\right)(P_b - P_\infty) + \frac{R}{C}\dot{P}_b - \frac{2\sigma}{R} - 4\mu\frac{\dot{R}}{R}. \tag{4}$$

Here, C represents the speed of sound in the liquid and $\dot{P}_b$ is the time derivative of the pressure inside the cavity. For a more detailed description of the various available equations of motion, the reader is referred to literature.[15]

B. Mass balance

The cavity is filled with both noncondensable gas and vapor and it is modeled with the van der Waals equation of state,[16]

$$\left(P_g + P_v + \frac{a}{v^2}\right)(v - b) = R_g T, \tag{5}$$

where P_g is the partial pressure of the gas, P_v is the partial pressure of the vapor, a and b are the van der Waals constants, v is the molar volume, R_g is the gas constant, and T is the temperature inside the cavity. The initial composition of the cavity interior is calculated from Eq. (4), assuming that the cavity is in a quasistatic equilibrium and the vapor pressure equals its saturation value.

During cavity motion, gas diffuses into and out of the cavity. It is assumed that the transport rate of gas is determined by diffusion in a thin stagnant liquid film surrounding the cavity (Fig. 1). To describe the flux of gas molecules, $\dot{N}_g$ (mol/s), the Maxwell-Stefan diffusion model has been used,[17]

$$\dot{N}_g = 4\pi R^2 \frac{D_l}{\delta_g}\frac{C_s - C_i}{(C_l - (C_s + C_i/2))}. \tag{6}$$

Here, D_l represents the gas-liquid diffusion coefficient, C_l the molar liquid concentration, and C_s and C_i the gas saturation and interface concentration, respectively. The saturation concentration is considered constant and it is calculated from the hydrostatic pressure and the saturated vapor pressure. The gas content near the interface is coupled to the partial gas pressure inside the cavity using equilibrium thermodynamics. In the Appendix , the exact correlations and values employed for these and other physical parameters are given. The boundary layer thickness δ_g is calculated from the penetration depth using a characteristic time scale of the process dynamics,[11]

$$\delta_g = \sqrt{\frac{RD_l\pi}{\dot{R}}}. \tag{7}$$

During expansion and contraction of the cavity, molecules evaporate and condense at the interface. Several approaches have been employed in literature to calculate the flux and the corresponding vapor pressure, some of which are discussed below.

A first approximation is to assume that the flux of vapor molecules is determined by the rate of evaporation and condensation. Yasui applied the Hertz-Knudsen-Langmuir equation to describe nonequilibrium phase transition across the interface,[9,18,19]

$$\dot{N}_v = 4\pi R^2 \frac{\alpha_M/M_v}{\sqrt{2\pi R_g/M_v}}\left[\frac{P_{\mathrm{vsi}}}{\sqrt{T_{\mathrm{li}}}} - \frac{P_{\mathrm{vi}}}{\sqrt{T_i}}\right]. \tag{8}$$

Here, $\dot{N}_v$ represents the vapor flux in mol/s, M_v is the molecular mass of the vapor, P_{vsi} is the saturated vapor pressure at the liquid interface temperature T_{li} and P_{vi} is the vapor pressure at the cavity interface temperature T_i. The accommodation coefficient α_M represents the ratio of the molecules that are absorbed to the interface and condense or evaporate,

to the total number of molecules that hit the interface. Several values have been reported for the accommodation coefficient, ranging from 10^{-3} to 1 for various systems.[9,20]

Toegel *et al.* suggested that vapor transport is controlled by the rate of diffusion inside the cavity.[11] Assuming that the total molar concentration inside the cavity, C_t, is spatially uniform, the following expression is obtained from the Maxwell-Stefan theory, which holds for diluted as well as concentrated systems:

$$\dot{N}_v = 4\pi R^2 \frac{D_b}{\delta_m} C_t \frac{P_{\mathrm{vi}} - P_v}{(P_b - (P_{\mathrm{vi}} + P_v/2))}. \tag{9}$$

The vapor mole fractions are calculated from the corresponding partial vapor pressures. The Chapman-Enskog theory has been applied to estimate the binary diffusion coefficient, D_b, using a Lennard-Jones intermolecular potential function.[21] The boundary layer thickness δ_m is calculated from the penetration depth using a characteristic time scale of the process dynamics, and a minimum value is incorporated to avoid that the boundary layer exceeds a length comparable to the cavity radius,[11]

$$\delta_m = \min\left(\frac{R}{\pi}, \sqrt{\frac{RD_b\pi}{\dot{R}}}\right). \tag{10}$$

The model presented in this paper accounts for diffusion as well as nonequilibrium phase transition by means of a vapor transport continuity equation across the interface, i.e., Eq. (8) is set equal to Eq. (9).

C. Energy balance

The model is concluded with an energy balance, which has been derived from the first law of thermodynamics for an open system,[22]

$$\dot{Q} - \dot{W} = -h_v\dot{N}_v - h_g\dot{N}_g + \frac{\mathrm{d}}{\mathrm{dt}}(N_g C_{pg} T + N_v C_{pv} T). \tag{11}$$

Here, h denotes the enthalpy per molecule, N is the number of vapor or gas molecules, and C_p represents the heat capacity. The enthalpy per molecule is given by the number of degrees of freedom. The work done by the cavity, $\dot{W}$, is calculated from the interior pressure and volume change. Heat conduction is chosen as the prevailing mechanism for heat transfer,

$$\dot{Q} = 4\pi R^2 \kappa_b \frac{T_i - T}{\delta_b}, \quad \delta_b = \min\left(\frac{R}{\pi}, \sqrt{\frac{R\alpha\pi}{\dot{R}}}\right). \tag{12}$$

Here, κ_b and α represent the thermal conductivity and diffusivity of the cavity interior, respectively. The kinetic theory of gases predicts that a temperature jump exists at the interface.[23] The interface temperatures in the liquid and the cavity can be correlated using

$$T_{\mathrm{li}} = T_i + \frac{1}{2kn}\sqrt{\frac{\pi\bar{M}}{2kT_i}}\frac{2 - a'\alpha_e}{\alpha_e}\kappa_b\frac{T_i - T}{\delta_b}. \tag{13}$$

Here, k represents the Boltzmann constant, n is the number density of the bubble interior, $\bar{M}$ is the mean mass of a molecule, a' is a constant, and α_e is the thermal accommodation coefficient.[9] The thermal accommodation coefficient represents the probability that a molecule, which hits the interface, reaches thermal equilibrium with the other phase.

Analogous to the vapor flux continuity equation, the energy fluxes across the interface are expressed in a conservation law. Taking phase transition, heat conduction, and the temperature jump into account, the following expression emerges:

$$4\pi R^2 \kappa_l \frac{T_l - T_{\mathrm{li}}}{\delta_l} = 4\pi R^2 \kappa_g \frac{T_l - T}{\delta_b} + \dot{N}_v \Delta H_{\mathrm{vap}} + (\dot{N}_v C_{pv} + \dot{N}_g C_{pg})(T_i - T_{\mathrm{li}}). \tag{14}$$

Here, κ_l is the thermal conductivity of the liquid, T_l is the liquid bulk temperature, and ΔH_{vap} represents the enthalpy of vaporization and condensation.

D. Numerical method

MATHEMATICA software has been used to solve the system of ordinary differential and algebraic equations, i.e., Eqs. (4), (6), (8), (9), (11), and (13).[24] The selected algorithm is based on a backward differentiation formula and Newton iterative methods.

The ordinary differential equations have been solved using appropriate initial conditions. It is assumed that initially the cavity radius equals R_0 and the cavity wall is at rest (i.e., $R=0$). Furthermore, the vapor pressures equal the saturated vapor pressure and the various temperatures equal the bulk liquid temperature. The initial number of vapor molecules in the cavity, $N_v(0)$, is calculated from the saturated vapor pressure and the initial number of gas molecules, $N_g(0)$ from the quasi-static assumption.

A demonstration version of the model is available in Ref. 36.

III. RESULTS AND DISCUSSION

First, the model is applied to describe cavitation in water saturated with argon to assist in the interpretation of the results obtained for liquid CO_2. Unless stated otherwise, the following base case conditions have been applied for these systems: $R_0=10$ μm, $f=20$ kHz, $\alpha_{\mathrm{M}}=0.4$, and $\alpha_{\mathrm{e}}=0.6$.[9,25,26]

A. Cavitation in aqueous systems

The cavity is set into radial motion by the forces acting on its wall. The driving force for motion is the sum of all these forces, i.e., $P_l - P_\infty$. At the onset of the rarefaction phase, the acoustic pressure of the applied sound field causes the driving force to exceed zero resulting in an expansion of the cavity (Fig. 2).

When the driving force equals zero [Fig. 2(a), point A] the cavity wall stops accelerating and a point of inflection is observed in the radius-time curve (point B). Although after this point $P_l - P_\infty$ turns negative, cavity expansion continues for several microseconds due to inertia effects, until a maximum radius is observed (point C). Hereafter, the negative

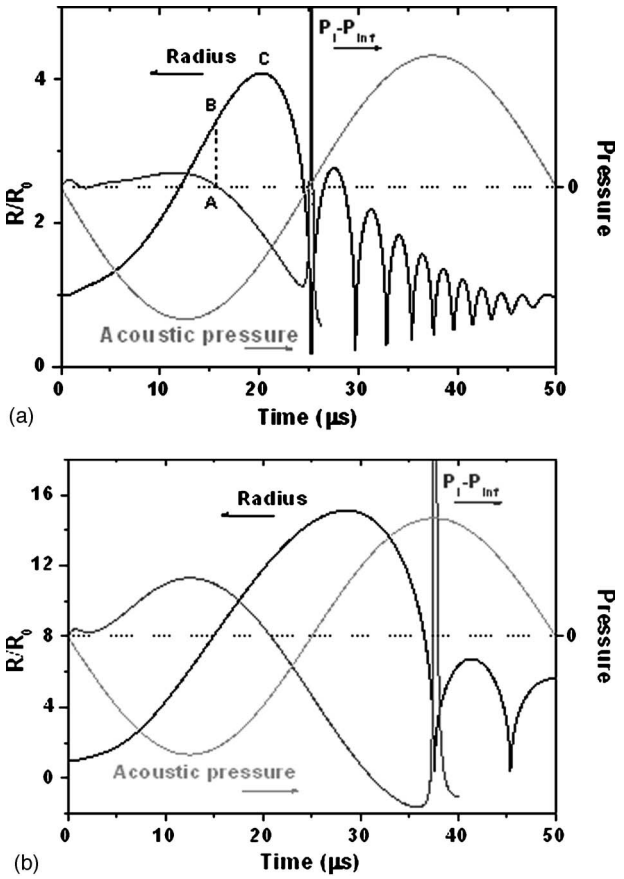

FIG. 2. Normalized radius-time curve (–), total pressure force P_l-P_{inf} (–), and acoustic pressure (–) for an argon cavity in water (P_h=10^5 N/m^2, T_l=293 K). (a) P_a=1.2×10^5 N/m^2 and (b) P_a=2.0×10^5 N/m^2.

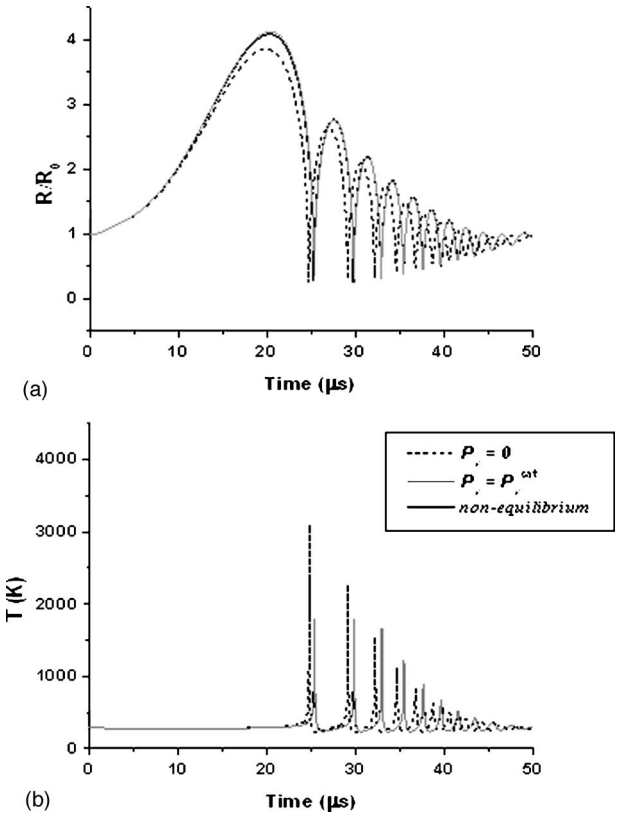

FIG. 3. Effect of vapor transport description on predicted normalized radius-time curve (a) and cavity interior temperature (b) for an argon cavity in water (P_h=10^5 N/m^2, T_l=293 K, P_a=1.2×10^5 N/m^2).

value of $P_l - P_\infty$ causes compression of the cavity. The driving force has accumulated from A to C. In addition, gas diffusion into and out of the cavity is relatively slow as compared to the cavity dynamics. Consequently, the pressure inside the large cavity has decreased significantly at C, resulting in a high driving force for compression compared to the driving force observed during expansion. Due to force accumulation and the low internal pressure, the cavity is set into a nonlinear motion and the collapse is relatively fast compared to the expansion. The sharp increase in $P_l - P_\infty$ marks the collapse of the cavity. Subsequently, the cavity oscillates several times until the rarefaction phase of the acoustic field sets in again and a new cavitation cycle starts. During this after bounce, the motion of the cavity roughly approaches the resonance or Minnaert frequency.[27]

Note that the implosion of the cavity can occur before that the applied sound field turns compressive. For higher acoustic pressures, point A moves to the right and in addition liquid inertia effects become more pronounced. Consequently, the onset of collapse is delayed and the implosion can occur during the compression cycle of the sound wave [Fig. 2(b)].

In the preceding analysis, the effect of vapor transport on process dynamics has been omitted in the discussion. However, during expansion the vapor pressure inside the cavity decreases below its saturation value and consequently molecules evaporate from the liquid into the cavity. Conversely, during compression the vapor pressure exceeds its saturation value and hence condensation will occur at the cavity wall. The importance of vapor transport is demonstrated by numerical simulations for two hypothetical cases: no vapor pressure (P_v=0) and thermodynamic equilibrium (P_v=P_{vs}). In addition, more physically realistic simulations have been carried out in which mass transfer limitations are incorporated using the vapor transport continuity equation across the interface, as discussed in Sec. II B (*nonequilibrium*). The results are depicted in Fig. 3.

First of all, Fig. 3(a) shows that the presence of vapor in the cavity results in an expansion to a larger maximum radius. This is due to the additional interior pressure force. During expansion, the evolution of the radius in time is almost similar for the hypothetical case P_v=P_v^{sat} and the nonequilibrium simulation. Furthermore, the cavity expands isothermally [Fig. 3(b)]. These observations indicate that the expansion occurs at conditions close to thermodynamic equilibrium. Upon collapse the process dynamics are fast with respect to mass and heat transfer leading to an almost adiabatic compression of the cavity interior, resulting in a sharp local temperature increase. The obtained temperature is predominantly determined by the cavity contents and the corresponding specific heat capacity. For the hypothetical case that the cavity is solely filled with Ar, P_v=0, the number of molecules present upon collapse and the heat capacity are relatively low, which leads to the most efficient heating. Since water vapor has a higher heat capacity compared to Ar, and due to the additional number of vapor molecules in the

TABLE I. Relevant physicochemical properties of water and liquid CO_2 (Refs. 28 and 29).

Property	Water (293 K, 10^5 N/m^2)	CO_2 (288 K, 52×10^5 N/m^2)
ρ (kg m^{-3})	998	825
μ (Pa s)	1×10^{-3}	7×10^{-5}
C (m s^{-1})	1483	394
P_{vs}(N m^{-2})[a]	2×10^3	51×10^5
σ (N m^{-1})[a]	72×10^{-3}	2×10^{-3}

[a]Saturation values.

cavity, the adiabatic compression is less efficient for the hypothetical case $P_v=P_v^{sat}$ and a smaller temperature increase is predicted. During the collapse, diffusion and condensation of water vapor are relatively slow and vapor is trapped in the cavity interior. Consequently, the effect as observed for the hypothetical case $P_v=P_v^{sat}$ is reinforced in the nonequilibrium situation and the temperature increase is at its lowest.

B. Cavitation in liquid carbon dioxide

The distinct physicochemical properties of liquid CO_2 may influence the cavity dynamics to a large extent (Table I). The effect of the elevated vapor pressure is considered to be most pronounced. In contrast to aqueous systems, the relative contribution of the vapor pressure to the driving force is large for liquid CO_2 and a deviation in its value may have a pronounced effect on cavity dynamics. For instance, due to vapor transport limitations during compression, the vapor pressure can exceed its saturation value causing cushioning of the collapse and "softer" cavitation.

The numerical simulations demonstrate that acoustic cavitation in liquid CO_2 is hindered for conditions similar to those which induce nonlinearity in water (Fig. 4). The cavity radius hardly increases and consequently no sharp temperature increase is observed.

At the beginning of the rarefaction phase, the negative acoustic pressure induces a driving force for radial motion, i.e., P_l-$P_\infty>0$, leading to cavity expansion (Fig. 5). This increase in cavity radius is accompanied by a sharp decrease in interior vapor pressure and hence an increase in P_{vs}-P_v.

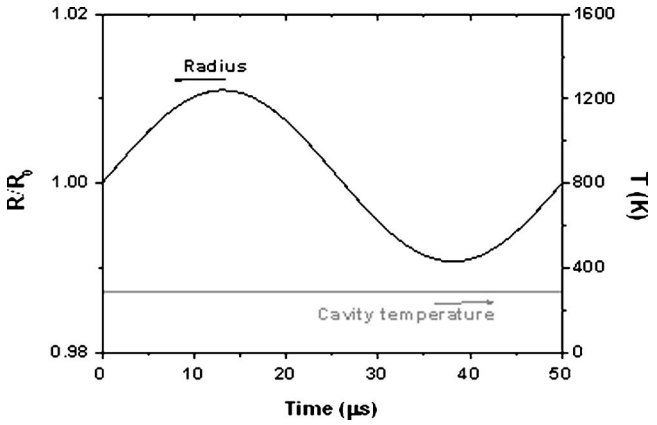

FIG. 4. Normalized radius-time curve (–) and interior temperature (–) for a cavity in liquid CO_2 saturated with argon ($P_h=52\times10^5$ N/m^2, $T_l=288$ K, $P_a=1.2\times10^5$ N/m^2).

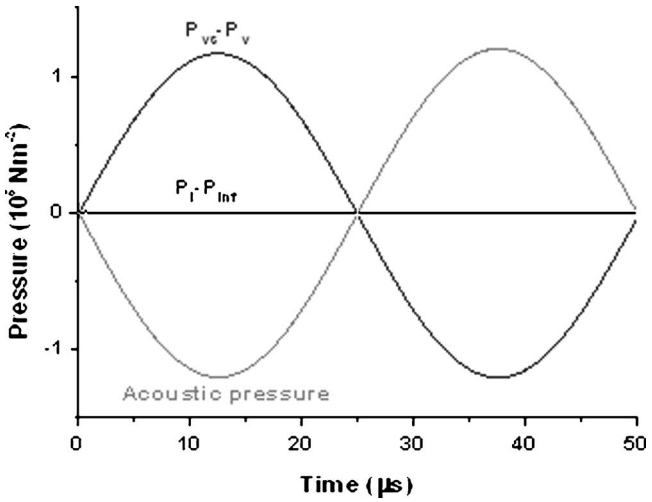

FIG. 5. Total pressure force P_l-P_{inf} (–), acoustic pressure (–), and saturated vapor pressure minus cavity vapor pressure P_{vs}-P_v (–) for a cavity in liquid CO_2 saturated with argon ($P_h=52\times10^5$ N/m^2, $T_l=288$ K, $P_a=1.2\times10^5$ N/m^2).

Due to the substantial contribution of the vapor pressure to the cavity interior pressure, a small deviation in this pressure strongly affects the driving force and the cavity dynamics. The reduction in pressure slows down the cavity, which impedes inertia effects. As a result, acceleration of the cavity wall and an increase of the interior temperature are not observed.

In contrast to cavitation in aqueous systems, these results suggest that vapor transport limitations considerably affect cavity expansion in liquid CO_2. To investigate the exact cause of the decrease in interior vapor pressure, numerical simulations have been performed for two hypothetical cases: absence of vapor transport limitations ($P_v=P_{vs}$) and absence of heat transport limitations ($T=T_l$). In practice, this implies that for the respective simulations the vapor transport coefficients, α_M and D_b, and the heat transport coefficients, κ_l and κ_g, are increased by a factor of 10^5. The results for the two hypothetical cases are depicted in Fig. 6.

Even in the limiting case that vapor transport limitations are absent, the vapor pressure inside the cavity decreases

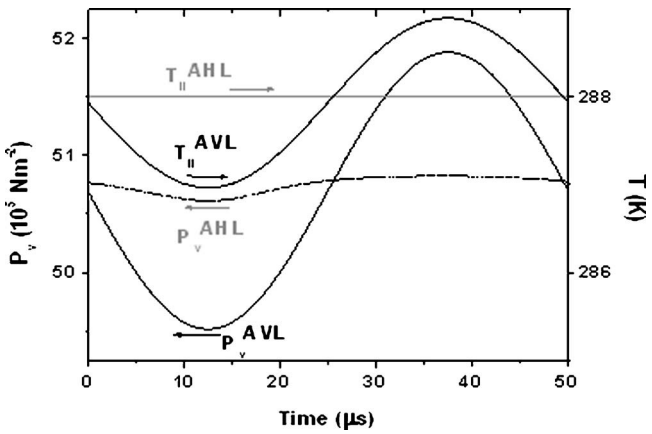

FIG. 6. Evolution of vapor pressure and liquid interface temperature for a cavity in liquid CO_2 saturated with argon in the absence of vapor transport limitations (–) and in the absence of heat transport limitations (–) ($P_h=52\times10^5$ N/m^2, $T_l=288$ K, $P_a=1.2\times10^5$ N/m^2).

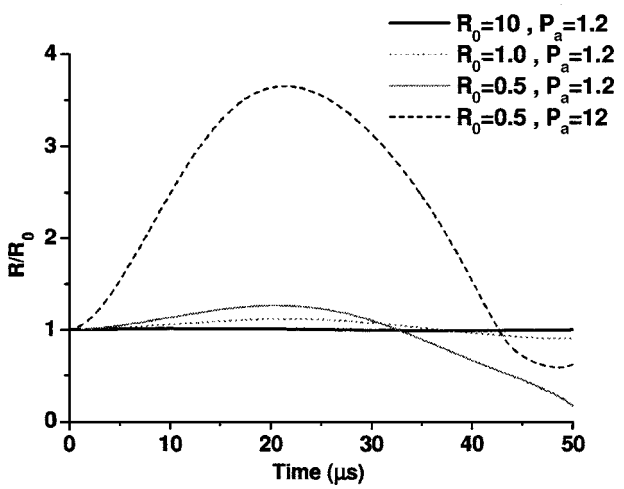

FIG. 7. Effect of initial radius (μm) and acoustic pressure (10^5 N/m^2) on predicted normalized radius-time curve for a cavity in liquid CO_2 saturated with argon ($P_h=52\times10^5$ N/m^2, $T_l=288$ K).

significantly. This suggests that the inhibition of cavity growth does not solely arise from vapor transport limitations. Due to the high vapor pressure of CO_2, a high flux of vapor molecules is required to maintain dynamic equilibrium during expansion, and a large amount of energy has to be supplied to facilitate the corresponding phase transition of the CO_2 molecules. Because the transfer of energy from the liquid is slow compared to the cavity dynamics, the temperature at the interface decreases (Fig. 6). The strong temperature dependency of the saturated vapor pressure of liquid CO_2 forces the vapor pressure at the interface to decrease well below its saturation value at the bulk liquid conditions. As a result, the driving force for vapor transport diminishes [Eq. (8)] and the cavity interior pressure decreases.

To check the effect of heat transfer limitations, simulations have been performed in which the heat transfer coefficients are increased by a factor of 10^5. Even though the interface temperature remains constant, the interior vapor pressure decreases due to vapor transport limitations. This suggests that both heat and vapor transports impede nonlinear cavitation dynamics in liquid CO_2. The decrease in vapor pressure is less pronounced compared to the hypothetical case $P_v=P_{vs}$, and this indicates that the effect of heat transport limitations is the most significant. Numerical simulations have shown that the effects encountered at low acoustic pressure are reinforced at higher driving pressures.

The lower surface tension of liquid CO_2 stabilizes smaller cavities against dissolution. For smaller cavities the volume to surface area ratio decreases, which implies that the effect of vapor and heat transport limitations will be less pronounced. To investigate if this results in nonlinear motion, numerical simulations have been performed for various initial radii and acoustic pressures (Fig. 7). These results demonstrate that for a smaller initial radius the cavity expands to a larger normalized radius. The rate of expansion is sufficient to induce inertia effects, which delay cavity compression. The involved driving force is largely counteracted by the decrease in vapor pressure, and therefore almost no force accumulates during this delay. As a result, the cavity wall is not accelerated and nonlinearity is not observed. The effects associated with the expansion phase also hold for the compression phase. Vapor and heat transport limitations slow down cavity contraction. It seems plausible to assume that these effects will be reinforced during nonlinear cavitation dynamics.

In conclusion, the presented simulations indicate that transport limitations oppose nonlinear radial motion in liquid CO_2. Although quantitative model predictions are complicated by the strong dependence of the physicochemical properties of CO_2 on temperature and pressure, the presented model qualitatively captures cavity dynamics in liquid CO_2.

IV. CONCLUSIONS

In this work, a single-cavity dynamics model has been proposed to study the governing processes of acoustic cavitation in liquid CO_2. This model includes a momentum balance, an expression for vapor and gas transports, and an energy balance. For the description of mass transport, diffusion inside and outside the cavity as well as nonequilibrium phase transition is taken into account.

To aid interpretation of simulation results for cavity dynamics in liquefied CO_2, the model has first been used to describe cavitation in water at ambient conditions. The simulations show that in water inertia effects and force accumulation can lead to a nonlinear radial motion of the cavity. Especially during collapse, the radial motion can be relatively fast compared to heat and mass transfer, resulting in an almost adiabatic compression of the cavity interior manifested by a sharp local pressure and temperature increase. Due to relatively slow transport, water vapor is trapped in the cavity interior during collapse, resulting in a lower temperature rise.

Numerical simulations have shown that cavitation in liquid CO_2 is impeded by mass and heat transport limitations. The transport limitations can already influence radial motion during the expansion phase, where the increase of volume is accompanied by a significant decrease of the pressure inside the cavity. This decrease in pressure slows down the expansion of the cavity. As a result, inertia effects and force accumulation become less pronounced and nonlinear motion is not observed. Simulations have indicated that the pressure decrease arises from heat transfer limitations rather than from mass transfer limitations. Heat transfer limitations allow a temperature decrease of the cavity wall, which corresponds to a decrease in vapor pressure.

NOMENCLATURE

a = van der Waals constant [J m^3/mol^2]
A = cavity surface area [m^2]
a' = arbitrary parameter [$\cdots$]
b = van der Waals constant [m^3/mol]
C = speed of sound in the liquid [m/s]
C_i = gas interface concentration [mol/m^3]
C_l = molar liquid concentration [mol/m^3]
C_{pg} = specific heat capacity gas [J/mol K]
C_{pv} = specific heat capacity vapor [J/mol K]
C_s = gas saturation concentration [mol/m^3]

C_t = total molar concentration [mol/m^3]
D_b = vapor diffusion coefficient [m^2/s]
D_l = gas-liquid diffusion coefficient [m^2/s]
e = energy per unit mass [J/kg]
f = ultrasonic frequency [Hz]
h_g = enthalpy per gas molecule [J]
h_v = enthalpy per vapor molecule [J]
ΔH_{vap} = enthalpy of vaporization and condensation [J/mol]
k = Boltzmann constant [m^2 kg/s^2 K]
$\bar{M}$ = molecular mean mass [kg]
M_g = molar mass gas [kg/mol]
M_v = molar mass vapor [kg/mol]
n = number density [m^{-3}]
N_g = amount of gas [mol]
$\dot{N}_g$ = gas flux [mol/s]
N_v = amount of vapor [mol]
$\dot{N}_v$ = vapor flux [mol/s]
P_a = acoustic pressure [Pa]
P_b = cavity interior pressure [Pa]
P_g = partial gas pressure [Pa]
P_h = hydrostatic pressure [Pa]
P_l = pressure at the interface [Pa]
P_v = partial vapor pressure [Pa]
P_{vi} = vapor pressure at the interface [Pa]
P_{vs} = saturated vapor pressure at infinity [Pa]
P_{vsi} = saturated vapor pressure at the interface [Pa]
P_∞ = pressure infinitely far from the cavity [Pa]
$\dot{Q}$ = heat transfer [J/s]
R = cavity radius [m]
$\dot{R}$ = time derivative of the cavity radius [m/s]
$\ddot{R}$ = second time derivative of the cavity radius [m/s^2]
R_g = universal gas constant [J/mol K]
R_0 = initial radius [m]
t = time [s]
T = temperature bubble interior [K]
$\dot{T}$ = temperature change [K/s]
T_i = cavity temperature at the interface [K]
T_l = bulk liquid temperature [K]
T_{li} = liquid temperature at the interface [K]
v = molar volume [m^3/mol]
V = cavity volume [m^3]
$\dot{V}$ = volume change [m^3/s]
$\dot{W}$ = work performed by cavity [J/s]

Greek symbols

α = thermal diffusivity [m^2/s]
α_e = thermal accommodation coefficient [$\cdots$]
α_M = mass accommodation coefficient [$\cdots$]
δ_b = thermal boundary layer cavity interior [m]
δ_g = gas diffusion boundary layer thickness [m]
δ_l = thermal boundary layer liquid [m]
δ_m = vapor diffusion boundary layer thickness [m]
κ_b = thermal conductivity cavity interior [W/m K]
κ_l = thermal conductivity liquid [W/m K]
μ = dynamic viscosity [Pa s]
ρ_t = density [kg/m^3]
σ = surface tension [N/m]

APPENDIX: PHYSICAL PARAMETERS

The values of the physical parameters are obtained either from experimental data from literature or from pure component correlations.

The values for the liquid properties ρ_l, μ, C, C_{pl}, P_{vs}, κ_l, and D_l are determined at the bulk conditions, T_l and P_h, and these parameters are considered constant during an acoustic cycle. Since the temperature at the interface evolves during an acoustic cycle, the interface properties ΔH_{vap}, σ, and P_{vsi} are calculated as a function of the interface temperature T_{li}.

The temperature inside a cavity increases considerably during the collapse and temperature-dependent correlations are used for the cavity interior properties C_{pv}, κ_g, and κ_v. These low temperature correlations are extrapolated for higher temperatures. The mixture properties are calculated from pure component properties using a geometric combining rule with a quadratic dependence on mole fraction.[21] For an arbitrary parameter Q, this implies

$$Q_m = \sum_{i=1}^{n} \sum_{j=1}^{n} y_i y_j Q_{ij}, \quad Q_{ij} = \sqrt{Q_{ii} Q_{jj}}, \tag{A1}$$

in which the subscript m denotes the mixture property and i and j represent the pure component properties.

The binary diffusion coefficient D_{b0} is calculated from the Chapman-Enskog theory,[22]

$$D_{b0} = 7.2 \cdot 10^{-5} \frac{\sqrt{T((1/M_g) + (1/M_v))}}{\sigma_m^2 \Omega_D C_t}, \tag{A2}$$

where σ_m is the mixture characteristic length and Ω_D is the diffusion collision integral. The standard Lennard-Jones 12-6 potential is used for evaluating σ_m and Ω_D. The temperature dependency of the collision integral is incorporated by means of the Neufeld relation.[21] To correct for higher densities, the Enskog correction for dense gases is applied. The diffusion coefficient D_b is related to the low-density diffusion coefficient as follows:[30]

$$\frac{D_{b0}}{D_b} = \left(1 + \frac{2}{3} n_g \sigma_g^3 \left(\frac{\sigma_g + 4\sigma_v}{4\sigma_g + 4\sigma_v}\right) + \frac{2}{3} n_v \sigma_v^3 \left(\frac{\sigma_v + 4\sigma_g}{4\sigma_g + 4\sigma_v}\right)\right), \tag{A3}$$

where n_g and n_v represent the number densities of the gas and vapor, respectively, and σ_g and σ_v the characteristic lengths. A similar approach is employed for correcting the thermal conductivity of the cavity interior.

$$\kappa_b = \frac{b_m}{v}\left(\frac{1}{y} + 1.2 + 0.755y\right)\kappa_{b0}, \tag{A4}$$

where

$$y = \left(\frac{b_m}{v}\right) + 0.6250\left(\frac{b_m}{v}\right)^2 + 0.2869\left(\frac{b_m}{v}\right)^3 + 0.115\left(\frac{b_m}{v}\right)^4. \tag{A5}$$

Here, b_m is the mixture van der Waals constant, v is the molar volume, and κ_{b0} is the low-density thermal conductivity.

The values for ρ_l, μ, C, C_{pl}, P_{vs}, κ_l, and D_l are obtained from Ref. 28 for water. Second-order polynomials are fitted to literature data for the interface properties ΔH_{vap} and σ.[28] The saturated vapor pressure at the interface, P_{vsi}, is calculated as a function of the interface temperature using the Antoine equation.[21] The pure component van der Waals constants are obtained from Ref. 28 and the Lennard-Jones parameters from Ref. 21. The specific heat capacity of argon is set equal to $5/2\ R_g$, and the temperature-dependent correlation for the water vapor heat capacity is obtained from Ref. 21. The descriptions for the argon and water vapor thermal conductivity are obtained from Refs. 31 and 32, respectively. The gas concentrations in the liquid are determined from the corresponding pressures using Henry's law constant of $1.5 \cdot 10^{-5}$ mol/N m.[29]

For liquefied carbon dioxide, the properties ρ_l, μ, C, C_{pl}, P_{vs}, and κ_l are obtained from Ref. 29. The gas diffusion coefficient, D_l, is estimated from tracer diffusivity date and it is set to 2×10^{-8} m^2/s.[33] Temperature-dependent correlations for the interface properties ΔH_{vap}, σ, and P_{vsl} are taken from Ref. 34. For argon, the same correlations as those used for the water-argon system are applied. The van der Waals constants and the Lennard-Jones parameters of carbon dioxide are obtained from Refs. 28 and 21, respectively. The temperature-dependent expressions for the thermal conductivity and heat capacity of CO_2 vapor are acquired from Ref. 34. The gas concentrations are calculated from vapor-liquid equilibrium data, assuming a constant total molar concentration equal to the molar concentration of carbon dioxide.[35] The saturation concentration is determined at the hydrostatic pressure using reported bubble point pressures. For the interface concentration, a second-order polynomial is derived from the presented data, which describes the partial argon pressure as a function of liquid composition.

[1] K. S. Suslick, Science **247**, 1439 (1990).
[2] J. P. Luche, *Synthetic Organic Sonochemistry* (Plenum, New York, 1998).
[3] L. H. Thompson and L. K. Doraiswamy, Ind. Eng. Chem. Res. **38**, 1215 (1999).
[4] T. J. Mason and C. Petrier, in *Advanced Oxidation Processes for Water and Wastewater Treatment*, S. Parsons (IWA, London, 2004), p. 185.
[5] E. J. Beckman, J. Supercrit. Fluids **28**, 121 (2004).
[6] M. W. A. Kuijpers, D. van Eck, M. F. Kemmere, and J. T. F. Keurentjes, Science **298**, 1969 (2002).
[7] S. Balachandran, S. E. Kentish, R. Mawson, and M. Ashokkumar, Ultrason. Sonochem. **13**, 471 (2006).
[8] E. Riera, Y. Golás, A. Blanco, J. A. Gallego, M. Blasco, and A. Mulet, Ultrason. Sonochem. **11**, 241 (2004).
[9] K. Yasui, Phys. Rev. E **56**, 6750 (1997).
[10] B. Storey and A. Szeri, J. Fluid Mech. **396**, 203 (1999).
[11] R. Toegel, B. Gompf, R. Pecha, and D. Lohse, Phys. Rev. Lett. **85**, 3165 (2000).
[12] L. Rayleigh, Philos. Mag. **34**, 94 (1917).
[13] M. Plesset, J. Appl. Mech. **16**, 277 (1949).
[14] J. B. Keller and M. Miksis, J. Acoust. Soc. Am. **68**, 628 (1980).
[15] M. P. Brenner, S. Hilgenfeldt, and D. Lohse, Rev. Mod. Phys. **74**, 425 (2002).
[16] P. W. Atkins, *Physical Chemistry*, 6th ed. (Oxford University Press, Oxford, 1998).
[17] J. A. Wesselingh and R. Krishna, *Mass Transfer in Multicomponent Mixtures* (Delft University Press, Delft, 2000).
[18] S. Fujikawa and T. Akamatsu, J. Fluid Mech. **97**, 481 (1980).
[19] V. P. Carey, *Statistical Thermodynamics and Microscale Thermophysics* (Cambridge University Press, Cambridge, 1999).
[20] G. F. Puente and F. J. Bonetto, Phys. Rev. E **71**, 056309 (2005).
[21] B. E. Poling, J. M. Prausnitz, and J. P. O'Connell, *The Properties of Gases and Liquids*, 5th ed. (McGraw-Hill, London, 2001).
[22] R. B. Byron, W. E. Stewart, and E. N. Lightfoot, *Transport Phenomena*, 2nd ed. (Wiley, London, 2001).
[23] M. N. Kogan, *Rarefied Gas Dynamics* (Plenum, New York, 1969).
[24] MATHEMATICA, Wolfram Research Inc., 1993.
[25] B. Barber and S. Putterman, Phys. Rev. Lett. **69**, 3839 (1992).
[26] M. Zientara, D. Jakubczyk, G. Derkachov, K. Kolwas, and M. Kolwas, J. Phys. D **38**, 1978 (2005).
[27] T. G. Leighton, *The Acoustic Bubble* (Academic, London, 1994).
[28] D. R. Lide, *Handbook of Chemistry & Physics*, 87th ed. (CRC, Boca Raton, FL, 2006).
[29] P. J. Linstrom and W. G. Mallard, Eds., NIST Chemistry WebBook, NIST Standard Reference Database Number 69, National Institute of Standards and Technology, Gaithersburg MD, 20899 (June 2005).
[30] J. O. Hirschfelder, C. F. Curtiss, and R. B. Bird, *Molecular Theory of Gases and Liquids* 4th ed. (Chapman and Hall, London, 1967).
[31] V. Kamath, A. Prosperetti, and F. Egolfopoulos, J. Acoust. Soc. Am. **94**, 248 (1993).
[32] Y. S. Touloukian, P. E. Liley, and S. C. Saxena, *Thermal Conductivity: Nonmetallic Liquids and Gases* (IFI/Plenum, New York, 1970).
[33] R. C. Robinson and W. E. Stewart, Ind. Eng. Chem. Fundam. **7**, 90 (1968).
[34] T. E. Daubert and R. P. Danner, *Physical and Thermodynamic Properties of Pure Compounds, Data Compilation* (Taylor and Francis, London, 2006).
[35] E. Sarashina and Y. S. Arai, J. Chem. Eng. Jpn. **4**, 379 (1971).
[36] http://www.chem.tue.nl/spd